© 2018. Published by The Company of Biologists Ltd | Journal of Cell Science (2019) 132, jcs219907. doi:10.1242/jcs.219907

TOOLS AND RESOURCES

SPECIAL ISSUE: RECONSTITUTING CELL BIOLOGY

The use of decellularised animal tissue to study disseminating cancer cells

James F. E. Grey[1,2], Alastair Campbell-Ritchie[1], Nicola M. Everitt[1], Alexander J. Fezovich[1,2] and Sally P. Wheatley[2,*]

ABSTRACT

Since the establishment of cell culture, common practice has been to grow adherent cells in 2D monolayers. Although cells behave completely differently when grown under these artificial conditions, the ease of 2D culturing has meant that this practice still prevails, and adopting conditions that more closely reflect the natural microenvironment has been met with substantial inertia. The alternative, animal models that mimic natural human physiology, are less accessible, strictly regulated and require licences and expensive facilities. Although transition from 2D to 3D cell culturing is gathering momentum, there is a clear need for alternative culturing methods that more closely resemble *in vivo* conditions. Here, we show that decellularised organs gleaned from discarded animal carcasses are ideal biomimetic scaffolds to support secondary tumour initiation *in vitro*. Further, we describe how to decellularise tissue and perform basic histochemistry and immunofluorescence procedures for cell and matrix detection. Cancer cell behaviour on this matrix is followed by way of an example. Because integration into the traditional work flow is easy and inexpensive, we hope this article will encourage other researchers to adopt this approach.

KEY WORDS: Cancer, Decellularisation, Metastasis

INTRODUCTION

Dissemination of metastatic tumours causes 90% of cancer-associated mortality across almost all cancer types. The efficacy of novel drugs that aim to eliminate cancer cells are typically assessed on cells grown in 2D culture, xenografts and patient-derived xenografts in rodents, prior to any clinical trial (Hingorani et al., 2005; Kariolis et al., 2014). Although animal models are superior to 2D monocultures in terms of imitating human biology, they are expensive and require strict adherence to ethical procedures. Between the extremes of animal models and 2D culture, alternatives do exist, but their applications have mostly been limited to regenerative medicine, primarily to study cutaneous wound healing and post-operative tissue regeneration and grafting (Chian et al., 2015; Fu et al., 2017; Piterina et al., 2009; Teo et al., 2017). For some time, stem cell researchers have used decellularised matrices (DCMs) with the primary goal of generating replacement organs by repopulation with cells (Somers et al., 2012; Abolbashari et al., 2016; Mußbach et al., 2016). Tissue development and cell differentiation is also being studied in a similar manner (Bruno et al., 2017; Underhill and Khetani, 2018). In the context of cancer biology, DCMs are being used to mimic complex niches that more closely resemble how tumours develop, such as in oral, breast and lung cancers; however, the number of researchers adopting this method is small (Colley et al., 2011; Xiong et al., 2015; Mishra et al., 2018). Here, we use a 3D system similar to one described previously by Xiong et al. (2015), but use DCMs generated from laboratory animal waste as the biomimetic scaffolds. This system has been used to study all aspects of primary and secondary tumour microenvironments in 3D, with emphasis on demonstrating its suitability for the analysis of cancer cell invasion.

RESULTS

Preparation and quality control of DCM lung tissue

The decellularisation procedure resulted in a tenfold reduction in rat lung dry tissue weight (e.g. 130 mg native weight to 10–15 mg decellularised weight); thus, we estimate that the extracellular matrix (ECM) constitutes ∼10% of this organ (Fig. 1A). Tissue was cut uniformly into discs of 6 mm diameter using a borer (Fig. 1B). Discs varied in depth depending upon where they were excised in the tissue (Fig. 1C): marginal (1 mm) or central (5 mm). The success of decellularisation was assessed by staining nuclear material with haemalum. This simple stain was combined with a periodic acid Schiff diastase stain (PAS-D) to ensure that glycosaminoglycans (GAGs) were retained. GAGs are key post-translational modifications that occur on ECM proteins and are required for their correct function. Sections of native lung were haemalum positive (blue dots) and PAS-D positive (pink), demonstrating the presence of nucleated cells and GAGs in the unprocessed lung (Fig. 2A). In the DCM, no haemalum staining was present (Fig. 2B), proving that all cells had been removed. PAS-D staining, however, remained comparable in intensity to the native tissue, demonstrating that GAGs were still present (Fig. 2E). Together, these markers indicate that successful decellularisation had been achieved and GAGs retained. The alveolar structures of the native lung were notably still visible and their porosity similar in the DCM, indicating that the integrity of the organ had been maintained (Fig. 2A,B). Liver tissue, which is rich in glycogen, was used as a control to ensure effective α-amylase-mediated catalysis of glycogen hydrolysis (Fig. 2C,D).

Association of breast cancer cells with rat lung DCMs

As the macroscopic structure of the lung had been preserved, but cellular material eliminated, we used this DCM to investigate the behaviour of metastasising cancer cells. The breast cancer cell lines MCF7 and MDA231 originate from pleural effusions and thus have past association with the lungs. These lines were therefore selected to test the biocompatibility of this lung-derived DCM. Cells were seeded onto DCM discs at a density of 2.5×10^4 cells/cm^2, placed in

[1]Faculty of Engineering, University of Nottingham, Nottingham NG7 2UH, UK. [2]Department of Biochemistry, School of Life Sciences, University of Nottingham, Nottingham NG7 2UH, UK.

*Author for correspondence (sally.wheatley@nottingham.ac.uk)

S.P.W., 0000-0002-9550-8979

Received 1 May 2018; Accepted 15 October 2018

Journal of Cell Science (2019) 132, jcs219907. doi:10.1242/jcs.219907

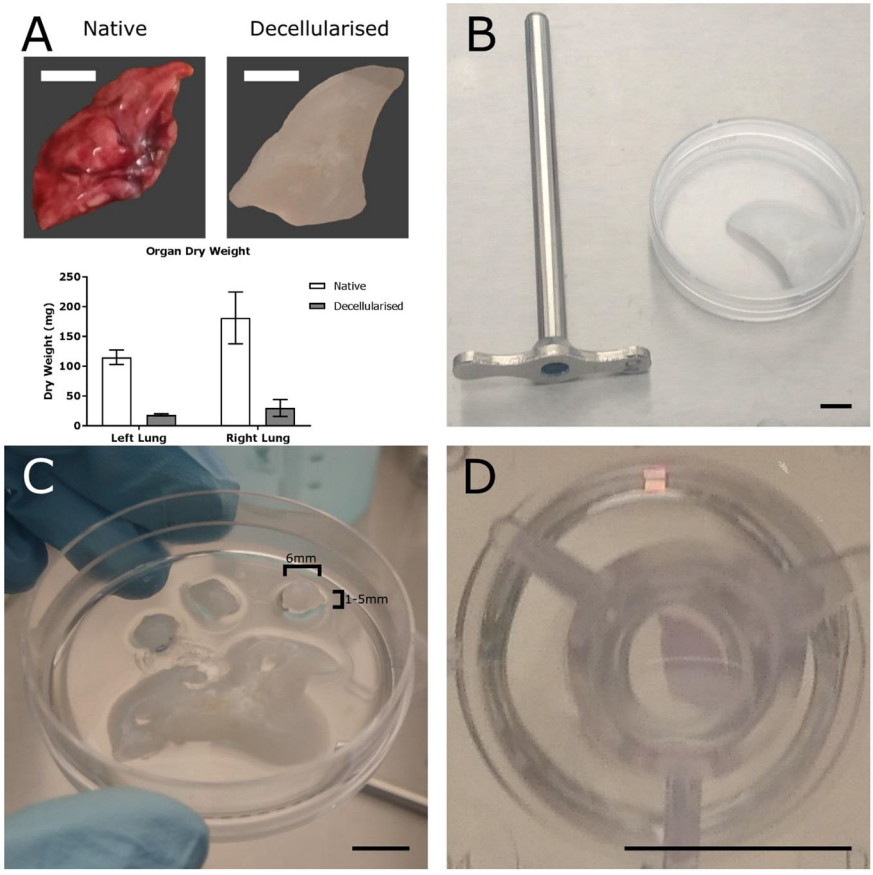

Fig. 1. Decellularisation work-flow. (A) Comparison of native and decellularised rat lung with respect to dry weight. (B) 6 mm diameter borer and decellularised lung. (C) 6 mm diameter DCM discs cut from tissue in B. (D) 6 mm diameter disc in 24-well plate insert. Scale bars: 10 mm.

well-inserts in a 24-well plate and submerged in medium (Fig. 1D). This configuration prevented cells from adhering to the plastic, thus confining their attachment to the DCM while still permitting nutrient exchange with the media. After 2 weeks in culture, samples were processed for histological analysis and then stained with PAS-D. Both cell lines adhered to the DCM, but their associations were markedly different (Fig. 3). MCF7 cells were present in clusters, both small and large, which appeared to become trapped in recesses within the matrix, but there was no evidence that they had invaded into the tissue (Fig. 3A–C). By contrast, individual MDA231 cells were found dispersed throughout the DCM, suggesting that they had actively migrated into it (Fig. 3D–F). In addition, MCF7 colonies stained positively with PAS-D, implying *de novo* synthesis of GAGs and thus the potential to remodel the matrix (Fig. 3B), whereas MDA231 cells were PAS-D negative, indicating that they do not make new ECM to facilitate their migration. We concluded that our system allows us to observe differences in MCF7 and MDA231 cell behaviour with the same substrate and that these differences are consistent with their behaviour *in vivo*.

ECM component preferences of breast cancer cells

Having established the compatibility of MCF7 and MDA231 cells with the DCM, we hypothesised that they might have preferences for different matrix components. To investigate this, areas rich in laminin-family proteins or collagen-I were highlighted by immunofluorescence staining. As expected, inspection of DCM alone identified the alveoli as laminin-rich structures (Fig. 4). Alveoli were successfully colonised by both MCF7 and MDA231 cells, suggesting that they both have affinity for laminin-rich substrate. By contrast, collagen I appeared less abundant in the matrix but was enriched in the pulmonary pleura and within decellularised blood vessel endothelium (Fig. 5). Interestingly, although MCF7 colonies populated these areas indiscriminately, MDA231 cells did not penetrate the collagen-rich areas of tissue nor did they populate the blood vessels, suggesting that collagen inhibits their invasion.

Assessment of proliferation cellular invasion into a DCM

To determine whether cellular proteins could be retrieved and analysed biochemically after growth on DCMs and whether cells were proliferative, samples containing MDA231 cells and DCM were sonicated in lysis buffer and the released proteins analysed by immunoblotting, with cells grown in 2D used as a reference (Fig. 6A,B). The presence of actin in the 3D sample demonstrates the efficacy of retrieval of cellular protein from the matrix, while, in the same blot, the lack of phosphorylated histone H3 (pH3) demonstrates that there was no cellular proliferation in the 3D sample. This was confirmed by Ki67 immunostaining, which showed ∼5% Ki67-positive MCF7 and MDA231 cells (Fig. S1), five- and tenfold lower than expected, respectively (Hollestelle et al., 2010).

Interestingly, when immunostained for the adhesion markers E-cadherin and cortactin, MCF7 cells were positive for both, whereas MDA231 cells were negative (Fig. 6C; Fig. S2).

To prove that our set-up is a suitable model for analysing metastasis, an invasion assay was carried out. Briefly, the matrix was seeded with 2.5×10^4 MDA231 cells and incubated for 7 days. Whole samples were then fixed, sectioned (5 µm slices) and a representative image acquired at 10× magnification with matrix edges acting as geographical coordinates. This enabled accurate measurement of migration distances for individual cells. As shown

Journal of Cell Science (2019) 132, jcs219907. doi:10.1242/jcs.219907

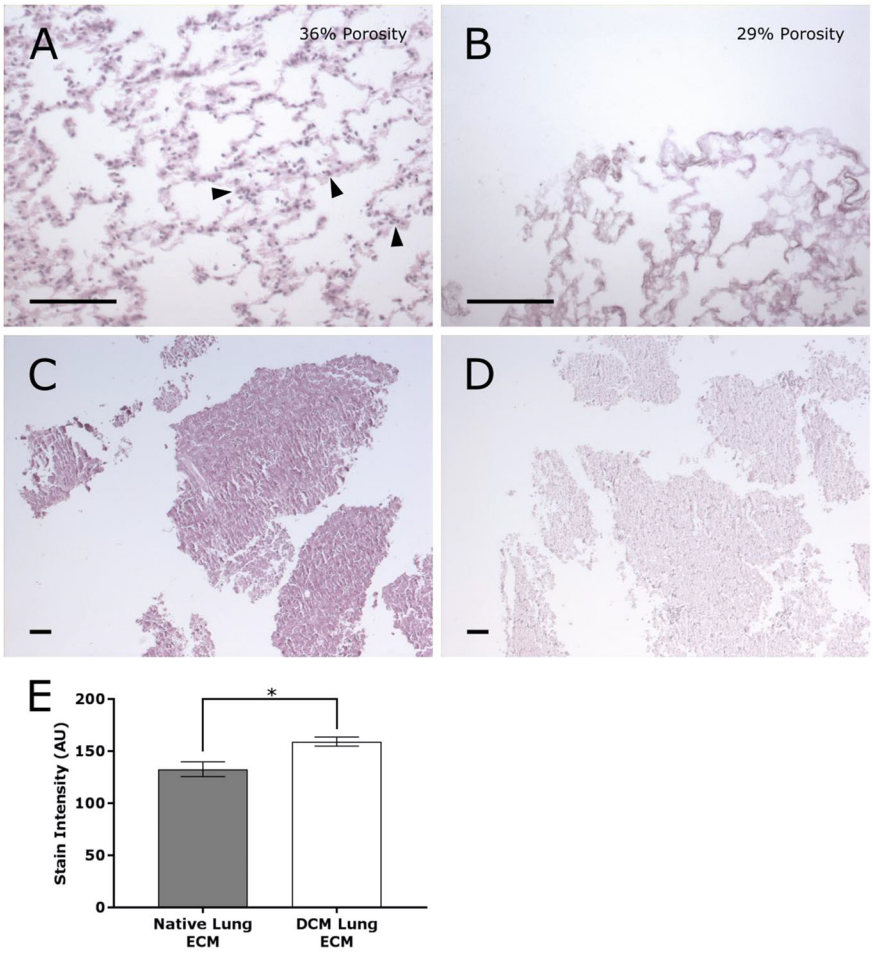

Fig. 2. Haemalum and PAS-D tissue staining of control samples. (A) Alveolar structures in α-amylase-treated native lung. (B) Alveolar structures in α-amylase-treated decellularised lung. Porosity was quantified using the BoneJ plug-in in Fiji. (C) Untreated native liver. (D) α-Amylase-treated native liver. (E) Stain brightness of native and decellularised lung ECM (*P=0.0451 by Welch's t-test). Nuclei are stained black, non-amino polysaccharides stained dark pink and amino polysaccharides stained pale pink. Arrowheads indicate nuclei. Scale bars: 100 µm. n=3 independent repeats.

in Fig. 6D,E, the majority of cells (~65%) only migrated up to 100 µm within 7 days. However, notably, some cells did penetrate the maximum distance achievable (400–450 µm) and, although small in number, this suggests the existence of a subset of highly motile pioneer cells within the population.

DISCUSSION

The number of 'waste' organs discarded in animal carcasses from laboratories throughout the world provides a huge opportunity to glean biomaterials for medical research and develop more realistic culturing methods to analyse cell behaviour. Importantly, if an

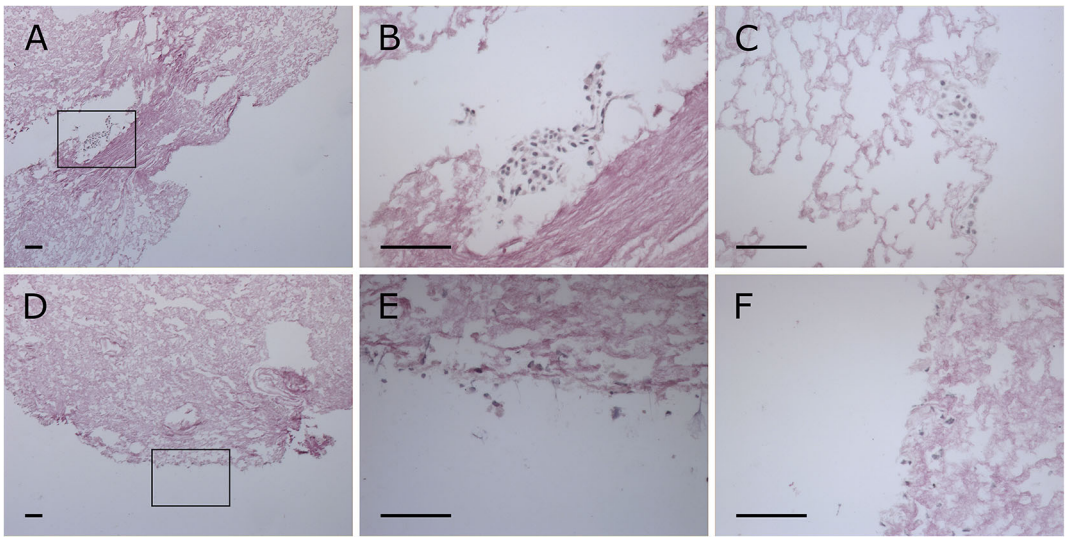

Fig. 3. Haemalum and PAS-D staining of MCF7 and MDA231 cells grown in decellularised lung. (A) Large MCF7 aggregate. (B) Zoom of boxed region shown in A. (C) Small MCF7^{casp3} aggregate. (D) MDA231 dispersion. (E) Zoom of boxed region shown in E. (F) MDA231 dispersion. Scale bars: 100 µm. n=3 independent repeats.

Journal of Cell Science (2019) 132, jcs219907. doi:10.1242/jcs.219907

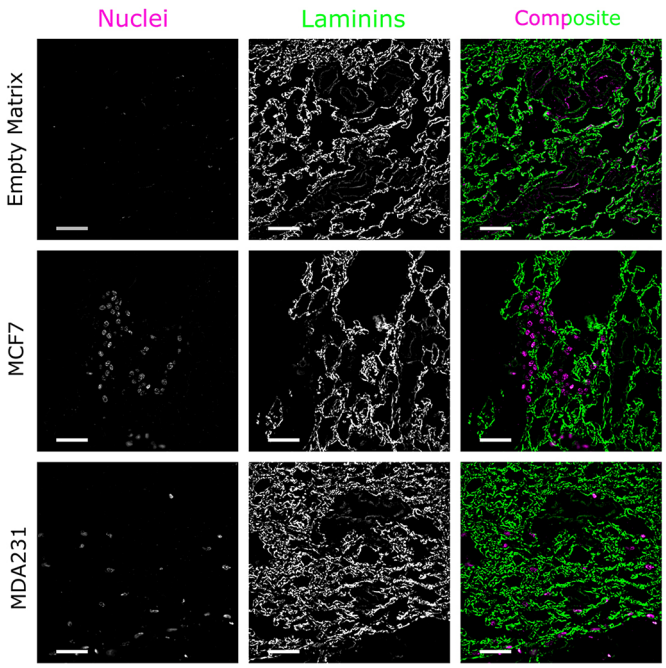

Fig. 4. Laminin-stained preparations of MCF7 and MDA231 cells grown on decellularised rat lung. Laminins retained after decellularisation throughout the laminin-rich alveoli. MCF7 aggregates occupied alveolar lumen, showing affinity for laminin-rich substrate. MDA231 cells widely dispersed into laminin-rich substrate. Scale bars: 50 µm. *n*=3 independent repeats.

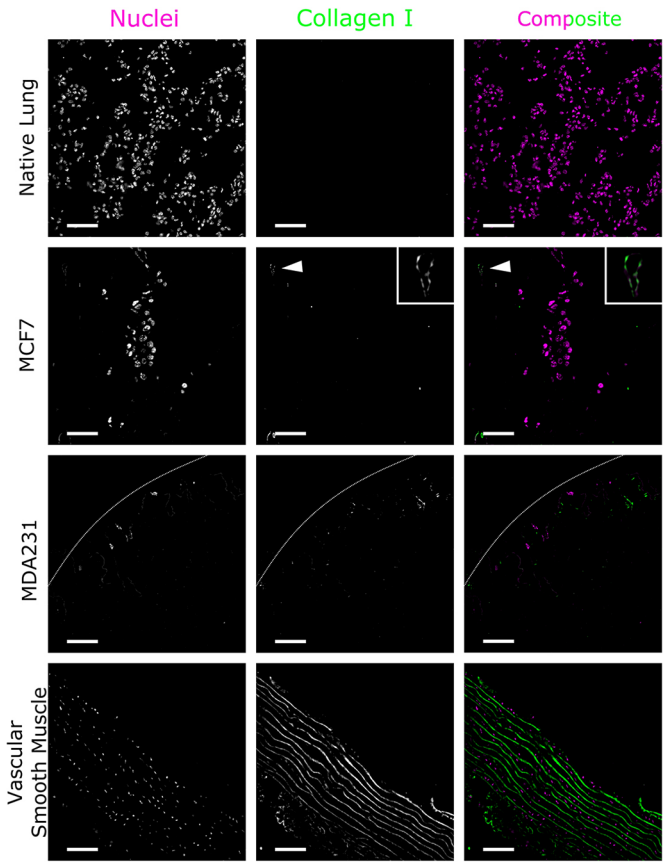

Fig. 5. Collagen I-stained preparations of MCF7 and MDA231 cells grown on decellularised rat lung. Empty matrix low in collagen I with mostly negative staining. MCF7 cells adjacent to a collagen I-rich blood vessel. MDA231 cells localised along the outside of the lung across collagen I-positive substrate. Arrowheads indicate enlarged areas. Vascular smooth muscle was used as a positive control. Line indicates edge of ECM. Scale bars: 50 µm. *n*=3 independent repeats.

animal has been used for the laboratory procedure for which it was procured, and ethical procedures followed, any part of the carcass can be used without the need for special licencing (at least in the UK). The simplicity of the decellularisation protocol used here, and the ease with which it can be integrated into traditional tissue culture practice, should encourage more researchers to steer away from traditional 2D monolayer cell culture and employ more natural culturing conditions. Moreover, although our preference was to use freshly prepared material for each experiment, if stored at 4°C in sterile PBS with antibiotics and antimycotics, matrices could be used up to 1 month after preparation with similar results (data not shown). For longer term storage, freeze drying (but not wet freezing) has been recommended when similar matrices have been used in other applications (Freytes et al., 2008).

To demonstrate its application, we compared the metastatic behaviour of two established breast cancer cell lines. Consistent with their origin as luminal tumour cells, the MCF7 cell line clusters during handling and readily forms organoids in culture (Neve et al., 2006). These cells are thought to metastasise primarily by dissociating from the matrix as a group, with weak responses to chemokines (Shields et al., 2007). In our system, the clustering behaviour of MCF7 cells was retained and these groups tended to become trapped in crevices and recesses within lung DCM. Furthermore, clustered MCF7 cells stained positive for PAS-D, suggesting that they were able to make new ECM to facilitate their migration in this environment. In contrast to MCF7 cells, the primary tumour from which MDA231 cells originated was categorised as 'Basal B' and metastasising MDA231 cells migrate as individuals, which is in line with previous research (Neve et al., 2006; Holliday and Speirs, 2011; Ivers et al., 2014; Xiong et al., 2015). Consistent with their nomadic behaviour *in vivo*, we observed solitary MDA231 cells invading deep into the lung DCM. We also noted that their invasion was inhibited by the presence of collagen I at the surface of the organ. This behaviour might reflect the fact that cancer cells with the same characteristics as MDA231 cells can metastasise to soft tissue unaided, but require the assistance of other cell types (such as osteoclasts and osteoblasts) to invade collagen-rich tissues such as bone (Wang et al., 2015). Given the differences in cell behaviour observed here, we believe that this system can be used to mimic the formation of secondary tumours by disseminating cancers of any origin. Further support for the use of DCMs to study cancer metastasis comes from Dunne et al. (2014), who compared cell behaviour on adipose-derived DCM with cells on matrigels or in xenografts, reporting that DCMs accurately mimicked the *in vivo* conditions.

To conclude, we describe how to make and use a simple and affordable cell culturing system that offers an alternative to standard 2D cell culture and more closely reflects the natural microenvironment that cells would encounter. Looking forward, the implementation of infrastructure within animal facilities to collect waste organs *en masse* could easily make available ample animal material for the cell biology community and would comply with the principles of NC3R: the replacement, refinement and reduction in the use of animals in medical research. Combined with internal quality control markers for specific tissue types, as exemplified here for lung ECM, this animal by-product represents an enormous resource for many biomedical applications.

Journal of Cell Science (2019) 132, jcs219907. doi:10.1242/jcs.219907

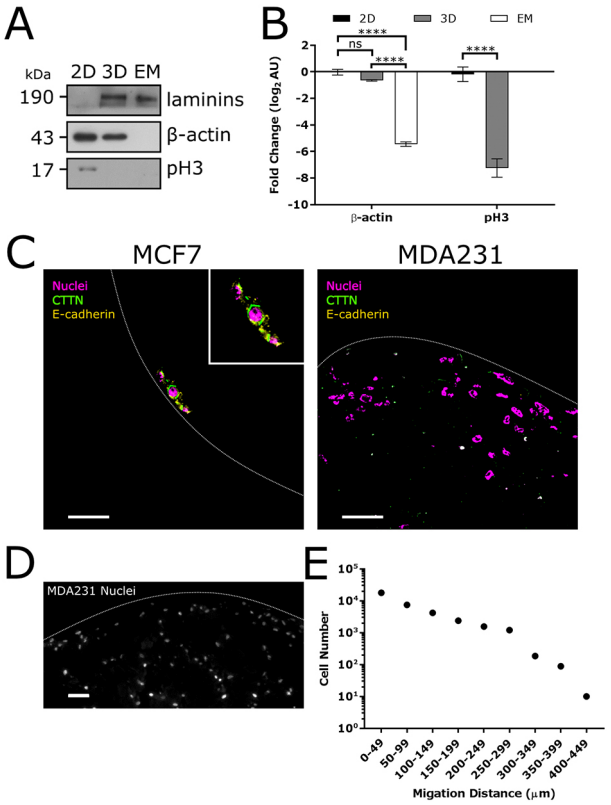

Fig. 6. Analysis of proliferation, adhesion and invasion in lung DCM. (A) Immunoblot for proliferation marker pH3. (B) Quantification of A, ****P<0.0001. (C) Immunohistochemical staining for cortactin (green) and E-cadherin (yellow). (D) Representative image of MDA231 invasion into lung DCM; cell nuclei stained with DAPI. Thin white lines indicate the DCM edge. (E) Quantification of invasion by MDA231 into lung DCM (N=34,986 cells; n=3 independent repeats), binned to 50 µm and plotted on a logarithmic scale. Scale bars: 50 µm.

MATERIALS AND METHODS

Preparation of DCM tissue discs

Whole organs were resected from waste rat carcasses immediately post-sacrifice and decellularised using the immersion protocol developed by A. Atala (2002, United States Patent No. 6376244). Harvested lungs (or liver) were immersed in sterile distilled water for 48 h to lyse cells osmotically. All steps were performed at 4°C in sterile glass bottles. Immersed organs were stirred at 200–300 rpm with a 10 mm magnetic stirrer. For each rat lung (~400 mg wet mass), a 500 ml volume was used and replaced once half-way through the process. Cellular debris was removed by immersing the tissue in clearing buffer (0.5% Triton X-100, 0.05% NH_4OH). The sample was rewashed with distilled water for 24 h to remove excess buffer and debris. Once decellularised (Fig. 1A), sections of 6 mm diameter were cut using a sterile stainless-steel metal borer (Fig. 1B,C) and equilibrated for 24 h in Dulbecco's modified PBS containing 1% penicillin/streptomycin (Sigma-Aldrich) (Fig. 1D).

Animal tissues were obtained from a tissue-sharing scheme at the University of Nottingham. The experiments for which animals were originally used were approved by the local animal ethical review board and rats were bred under a project licence granted under the UK Animals (Scientific Procedures) Act 1986, which incorporates Council Directive 2010/63EU of the European Parliament.

Cell culture

Two breast cancer cell lines were used: MCF7 (Jänicke et al., 1998) and MDA231. Cells were seeded at 2.5×10^4 cells/cm^2 onto 6 mm decellularised lung discs, suspended in a 24-well plate insert (Greiner Bio-One, 662630) and cultured in Dulbecco's modified Eagle's medium (Sigma-Aldrich, D6429) with 10% (v/v) foetal calf serum (Gibco). Cultures were incubated under standard conditions (37°C, 5% CO_2, with humidity) for 2 weeks before being processed for histology. During the incubation, the medium was replenished once in week 1 and twice in week 2.

Retrieval of cellular material from matrices

Matrices were seeded with 2.5×10^4 cells and cultured for 7 days as described. Samples were transferred into ice-cold PBS, washed and incubated on ice for 5 min. Samples were then transferred into Tris-Triton lysis buffer [100 mmol/l NaCl, 10 mmol/l Trizma, 1 mmol/l EDTA, 1 mmol/l EGTA, 10% glycerol (w/v), 1% Triton X-100 (v/v), 0.5% sodium deoxycholate (w/v), 0.1% SDS (w/v)] and incubated on ice with vigorous agitation. Finally, samples were sonicated three times at 20 Hz for 10 s, then centrifuged (500 ***g*** for 5 min at 4°C) and the pellet removed. Immunoblotting was performed by standard procedures and probed with 1:500 (1.36 µg/ml) anti-laminin antibody (Abcam, ab11575), 1:1000 anti-β-actin antibody (Sigma-Aldrich, A5315) or 1:500 anti-histone H3 (phospho-S10, Abcam, ab5176).

Histology

Samples were fixed in 4% formaldehyde in PBS for 15 min at room temperature, washed twice for 20 min in PBS and dH_2O before 20 min in dehydration washes with increasing concentrations of ethanol (70%, 95% and 100%), followed by three 20 min washes in xylene. All washes were carried out in 6 ml within 7 ml glass vials (Samco, T008/01). Samples were immersed in 50% paraffin in xylene at 64°C for 20 min before two final washes in 100% paraffin for 20 min at 64°C. Samples were set in a histological cassette (CellPath) overnight at room temperature and either stored at room temperature or sectioned (5 µm) using a Leica DSC1 microtome. Sections were deparaffinised by two 5 min washes in xylene followed by 5 min washes in reducing concentrations of ethanol (100%, 95% and 70%) with two final 5 min washes in dH_2O, in a filled Coplin jar. For staining, deparaffinised samples were treated with 0.5% (w/v) α-amylase (Sigma-Aldrich) for 30 min at 37°C, 0.5% periodic acid for 5 min at room temperature, followed by Schiff's reagent (Sigma-Aldrich) for 20 min at room temperature. Samples were counterstained with neat haemalum (ThermoScientific, LAMB-170-D) nuclear stain for 3 min at room temperature followed by a series of dehydration washes in increasing concentrations of ethanol (70%, 95% and 100%) and two washes in xylene, all for 5 min at room temperature. Finally, samples were mounted with distyrene plasticiser xylene (Sigma-Aldrich) mounting media. For immunological staining, deparaffinised samples underwent antigen retrieval by immersion in 10 mmol/l trisodium citrate solution (pH 6 with HCl) and microwaving on low power (ProLine, 750 W) for 20 min. Samples were blocked in blocking buffer [10% normal goat serum (v/v), 1% BSA (w/v) in TBST] for 1 h at room temperature, then probed overnight at 4°C with 1:100 (6.8 µg/ml) anti-laminin antibody (Abcam, ab11575), 1:100 (5 µg/ml) anti-collagen I antibody (Abcam, ab88147), 1:100 (5 µg/ml) anti-cortactin antibody (CST, 3502), 1:100 (5 µg/ml) anti-E-cadherin antibody (Abcam, ab76055) or 1:100 anti-Ki67 (Bio-Rad, AbD02531). Slides were washed three times in TBST for 5 min at room temperature before staining with the relevant secondary antibodies for 1 h at room temperature: 1:200 (750 µg/ml) fluorescein-conjugated anti-rabbit (Vector Laboratories) or 1:200 (750 µg/ml) fluorescein-conjugated anti-mouse (Vector Laboratories). All antibodies were diluted in blocking buffer. Finally, samples were counterstained with 1 µg/ml DAPI (Sigma-Aldrich, D9542) for 10 min at room temperature and mounted in Mowiol mounting medium (Sigma-Aldrich, 324590).

Imaging

Bright-field imaging was carried out using a Zeiss Axioplan microscope at 5× and 20× magnifications. Fluorescence imaging was performed on a DeltaVision Elite system at 20× magnification. Images were processed using Fiji software; bright-field images were white-balanced and processed in a fully automated manner.

Acknowledgements

We are grateful to the staff of the Bio-Support Unit at the University of Nottingham for facilitating the sharing of animal tissues and to Dr Rawan Hareeri for advice on dissections.

Competing interests
The authors declare no competing or financial interests.

Author contributions
Conceptualization: J.F.E.G., A.C.-R., N.M.E., S.P.W.; Methodology: J.F.E.G., A.C.-R., N.M.E., A.J.F.; Validation: J.F.E.G.; Formal analysis: J.F.E.G., A.J.F.; Investigation: J.F.E.G.; Resources: S.P.W.; Data curation: J.F.E.G., A.J.F.; Writing - original draft: J.F.E.G., S.P.W.; Writing - review & editing: J.F.E.G., N.M.E., A.J.F., S.P.W.; Visualization: J.F.E.G.; Supervision: A.C.-R., N.M.E., S.P.W.; Project administration: J.F.E.G., A.C.-R., N.M.E., S.P.W.; Funding acquisition: A.C.-R., N.M.E., S.P.W.

Funding
J.F.E.G. acknowledges a PhD studentship funded jointly by the University of Nottingham School of Life Sciences and Faculty of Engineering. A.J.F. is a Biotechnology and Biological Sciences Research Council (BBSRC)-DTP student.

Supplementary information
Supplementary information available online at
http://jcs.biologists.org/lookup/doi/10.1242/jcs.219907.supplemental

References

Abolbashari, M., Agcaoili, S. M., Lee, M.-K., Ko, I. K., Aboushwareb, T., Jackson, J. D., Yoo, J. J. and Atala, A. (2016). Repopulation of porcine kidney scaffold using porcine primary renal cells. *Acta Biomater.* **29**, 52-61.

Bruno, R. D., Fleming, J. M., George, A. L., Boulanger, C. A., Schedin, P. and Smith, G. H. (2017). Mammary extracellular matrix directs differentiation of testicular and embryonic stem cells to form functional mammary glands in vivo. *Sci. Rep.* **7**, 40196.

Chian, K. S., Leong, M. F. and Kono, K. (2015). Regenerative medicine for oesophageal reconstruction after cancer treatment. *Lancet Oncol.* **16**, e84-e92.

Colley, H. E., Hearnden, V., Jones, A. V., Weinreb, P. H., Violette, S. M., Macneil, S., Thornhill, M. H. and Murdoch, C. (2011). Development of tissue-engineered models of oral dysplasia and early invasive oral squamous cell carcinoma. *Br. J. Cancer* **105**, 1582-1592.

Dunne, L. W., Huang, Z., Meng, W., Fan, X., Zhang, N., Zhang, Q. and An, Z. (2014). Human decellularized adipose tissue scaffold as a model for breast cancer cell growth and drug treatments. *Biomaterials* **35**, 4940-4949.

Freytes, D. O., Tullius, R. S., Valentin, J. E., Stewart-Akers, A. M. and Badylak, S. F. (2008). Hydrated versus lyophilized forms of porcine extracellular matrix derived from the urinary bladder. *J. Biomed. Mat. Res. A* **87A**, 862-872.

Fu, H., Teng, L., Bai, R. Z., Deng, C., Lv, G. and Chen, J. (2017). Application of acellular intima from porcine thoracic aorta in full-thickness skin wound healing in a rat model. *Mat. Sci. Eng. C* **71**, 1135-1144.

Hingorani, S. R., Wang, L., Multani, A. S., Combs, C., Deramaudt, T. B., Hruban, R. H., Rustgi, A. K., Chang, S. and Tuveson, D. A. (2005). Trp53R172H and KrasG12D cooperate to promote chromosomal instability and widely metastatic pancreatic ductal adenocarcinoma in mice. *Cancer Cell* **7**, 469-483.

Hollestelle, A., Nagel, J. H. A., Smid, M., Lam, S., Elstrodt, F., Wasielewski, M., Ng, S. S., French, P. J., Peeters, J. K., Rozendaal, M. J. et al. (2010). Distinct gene mutation profiles among luminal-type and basal-type breast cancer cell lines. *Breast Cancer Res. Treat.* **121**, 53-64.

Holliday, D. L. and Speirs, V. (2011). Choosing the right cell line for breast cancer research. *Br. Cancer Res.* **13**, 215-221.

Ivers, L. P., Cummings, B., Owolabi, F., Welzel, K., Klinger, R., Saitoh, S., O'Connor, D., Fujita, Y., Scholz, D. and Itasaki, N. (2014). Dynamic and influential interaction of cancer cells with normal epithelial cells in 3D culture. *Cancer Cell Int.* **14**, 108.

Jänicke, R. U., Sprengart, M. L., Wati, M. R. and Porter, A. G. (1998). Caspase-3 is required for DNA fragmentation and morphological changes associated with apoptosis. *J. Biol. Chem.* **273**, 9357-9360.

Kariolis, M. S., Miao, Y. R., Jones, D. S., Kapur, S., Mathews, I. I., Giaccia, A. J. and Cochran, J. R. (2014). An engineered Axl "decoy receptor" effectively silences the Gas6-Axl signaling axis. *Nat. Chem. Biol.* **10**, 977-983.

Mishra, D. K., Miller, R. A., Pence, K. A. and Kim, M. P. (2018). Small cell and non small cell lung cancer form metastasis on cellular 4D lung model. *BMC Cancer* **18**, 441.

Mußbach, F., Settmacher, U., Dirsch, O., Xie, C. and Dahmen, U. (2016). Bioengineered livers: a new tool for drug testing and a promising solution to meet the growing demand for donor organs. *Eur. Surg. Res.* **57**, 224-239.

Neve, R. M., Chin, K., Fridlyand, J., Yeh, J., Baehner, F. L., Fevr, T., Clark, L., Bayani, N., Coppe, J.-P., Tong, F. et al. (2006). A collection of breast cancer cell lines for the study of functionally distinct cancer subtypes. *Cancer Cell* **10**, 515-527.

Piterina, A. V., Cloonan, A., Meaney, C., Davis, L., Callanan, A., Walsh, M. and Mcgloughlin, T. (2009). ECM-based materials in cardiovascular applications: inherent healing potential and augmentation of native regenerative processes. *Int. J. Mol. Sci.* **10**, 4375-4417.

Shields, J. D., Fleury, M. E., Yong, C., Tomei, A. A., Randolph, G. J. and Swartz, M. A. (2007). Autologous chemotaxis as a mechanism of tumor cell homing to lymphatics via interstitial flow and autocrine CCR7 signaling. *Cancer Cell* **11**, 526-538.

Somers, P., Robyns, L., Nollet, E., Somer, F., Cornelissen, M., Thierens, H. and Nooten, G. (2012). Platelet gel supernatant as a potential tool to repopulate acellular heart valves. *Cell Prolif.* **45**, 378-385.

Teo, L., Woo, Y. J., Kim, D. K., Kim, C. Y. and Yoon, J. S. (2017). Surgical outcomes of porcine acellular dermis graft in anophthalmic socket: comparison with oral mucosa graft. *Korean J. Opthalmol.* **31**, 9-15.

Underhill, G. H. and Khetani, S. R. (2018). Bioengineered liver models for drug testing and cell differentiation studies. *Cell. Mol. Gastroenterol. Hepatol.* **5**, 426-439.e1.

Wang, N., Reeves, K. J., Brown, H. K., Fowles, A. C., Docherty, F. E., Ottewell, P. D., Croucher, P. I., Holen, I. and Eaton, C. L. (2015). The frequency of osteolytic bone metastasis is determined by conditions of the soil, not the number of seeds; evidence from in vivo models of breast and prostate cancer. *J. Exp. Clin. Cancer Res.* **34**, 124.

Xiong, G., Flynn, T. J., Chen, J., Trinkle, C. and Xu, R. (2015). Development of an ex vivo breast cancer lung colonization model utilizing a decellularized lung matrix. *Integr. Biol.* **7**, 1518-1525.